Structural Trends and Vibrational Analysis of N,N,N′,N′-Tetramethylmalonamide Complexes Across the Lanthanide Series

Dmytro V. Kravchuk, Xiaoyu Wang, Michael J. Servis, Richard E. Wilson*

Chemical Sciences and Engineering Division, Argonne National Laboratory, Lemont, IL 60439 United States

Abstract

Fundamental understanding of coordination chemistry across the lanthanide series is essential for explaining chemical behavior of rare-earth metals in complex liquid-liquid extraction processes, which in turn affects the distribution ratios and efficacy of separations as a whole. In this work, we explore the structural trends between the lanthanides and a neutral N,N,N′,N′-tetramethylmalonamide (TMMA) ligand within four isolated families of solid-state compounds: Ln(*trans*-TMMA)$_2$(NO$_3$)$_3$ Ln = La-Nd, Sm; Ln(*cis*-TMMA)$_2$(NO$_3$)$_3$ Ln = Eu-Tb, Er; [Ln(TMMA)$_3$(NO$_3$)$_2$][Ln(TMMA)(NO$_3$)$_4$] Ln = Dy-Tm; Ln(K^2-TMMA)(iPrOH)(NO$_3$)$_3$ and Ln(K^1-TMMA)(K^2-TMMA)(NO$_3$)$_3$ Ln = Yb, Lu. Moving across the lanthanide series, we note the formation of both discrete charge-neutral complexes, as well as charged molecular anion-cation pairs, with variations in spatial ligand arrangement, coordination numbers, and ligand denticities. IR and Raman spectroscopy paired with DFT frequency analysis were used for an in-depth investigation of vibrational modes unique to each structural family. The collection of isolated model compounds was also discussed in the context of liquid-liquid separations based on reported distribution ratios from malonamide extraction.

Introduction

Current research efforts on the reprocessing of spent nuclear fuel focus on minimizing the radiotoxicity of the nuclear waste by separating the long-lived radionuclides by liquid-liquid extraction.[1] One such strategy to accomplishing this is by separation of trivalent actinide cations, Am(III) and Cm(III), from the trivalent lanthanide cations, Ln(III), in nitric acid by liquid-liquid extraction using diamides – the selective actinide extraction (DIAMEX-SANEX) process.[2] The DIAMEX-SANEX separation involves contacting the raffinate from the PUREX (plutonium uranium reduction extraction) process with a mixture of a malonamides (diamide) and a dialkylphosphoric acid dissolved in an aliphatic phase.[3] Under typical acidic conditions (~3M HNO_3), the malonamides successfully batch extract all of the Ln(III) and An(III) into the organic phase. Due to different acid concentration dependencies of solvating and cation exchange extraction mechanisms, when the loaded organic phase is contacted with a dilute aqueous solution of diethylenetriaminepentaacetic acid, the malonamide loses its extraction capacity, while the dialkylphosphoric acid preferentially binds to Ln(III), thus recovering the An(III) back into the aqueous phase.

From the perspective of f-element coordination chemistry, malonamides are of particular interest because they are neutral ligands that can successfully compete with coordinated aqua ligands for a binding site on the metal ion.[4] Numerous studies focused on improving the separation factors by modifying malonamides based on alkyl group substituents,[5] the conformation[6] and preorganizationof the ligand,[7] as well as variations to the carbon backbone in order to enhance binding affinity to the metal ion.[8] For example, Spjuth *et al*. demonstrated that various aliphatic and aromatic substituents on both the amide-N and the methylene-C of the malonamide-based extractant varies the basicity of the ligand, thus affecting the extraction of Am(III) and Eu(III) from the nitric acid media.[9] While Lumetta *et al*. considered how the conformational orientation of donor groups (*cis*, *trans*, or *gauche* of the neighboring C=O) affects the binding affinity of the malonamide ligand and suggested the bicyclic backbone modification.[7a] Such synthetic adjustment was later implemented by Parks *et al*. showing 10-

100 fold increase in binding affinity of the bicyclic malonamide extractant with Ln(III) compared to the acyclic counterpart.[7b] Finally, the molecular dynamics calculations paired with X-ray scattering techniques have been used by our group to study the effect of intermolecular interactions of the malonamide extractant on the solution nanostructure to gain a fundamental understanding of the energetics of the extraction process.[10]

Despite the demonstrated ability of malonamide based extractants to separate trivalent f-elements, a broad understanding of their coordination chemistry, in particular their structural properties in the solid and solution states remains underexplored, particularly as it relates to their structures across the entirety of the lanthanide series and spectroscopic signatures indicative of their solution structures. The commonly used diamide-based extractants such as N,N′-dimethyl-N,N′-dibutyltetradecylmalonamide (DMDBTDMA) or N,N′-dimethyl-N,N′-dioctylhex-ylethoxymalonamide (DMDOHEMA) are impractical for investigations of the solid-state lanthanide-diamide binding motifs due to the presence of long aliphatic alkyl chains.[11] Thus, the metal-diamide complexes are typically crystallized out with N,N′-substituted malonamides with methyl, ethyl, cyclohexyl, or phenyl as common substituents, e.g. N,N,N′,N′-tetramethylmalonamide (TMMA). Generally, the primary mode of malonamide binding is a bidentate (K^2) coordination to the metal center via both carbonyl oxygens (C=O) of the diamide functional group, as first shown by Castellano and Becker in 1981 in their $[La(K^2\text{-}TMMA)_4](PF_6)_3$ complex.[12] If the malonamide ligand contains a pair of secondary amides instead of a fully substituted tertiary analogue, it is possible to observe a rare μ_2-O,O′ bridging motif, where the C=O carbonyls take on the *trans* conformation and bridge two uranyl cations with the amide N-H engaging in hydrogen bonding with the uranyl oxo, as shown in $[(UO_2((C_6H_5CO)_2CH)_2)_2(\mu_2\text{-}(C_6H_5NHCO)_2CH_2)]$.[13]

While there are a reasonable number of solid-state structures reported for the lanthanide-malonamide complexes, there is a lack of a systematic study evaluating at the solid-state complexes across the lanthanide series as a whole. Herein we report the synthesis and characterization of four major families of lanthanide-N,N,N′,N′-tetramethylmalonamide complexes that are differentiated by the ligand

arrangement about the metal center, the denticity of the coordinated ligand, and the supramolecular assembly of charged molecular complexes across the entire lanthanide period. Keeping the same synthetic conditions in the reactions of lanthanides with N,N,N',N'-tetramethylmalonamide (TMMA) allowed us to systematically study how the trend of lanthanide contraction affects the structures of crystallized coordination compounds and the associated vibrational signatures. The structural trends we observe within the series of isolated Ln-TMMA model compounds could help explain the differences in extraction behavior of various lanthanides in the presence of diamide-based ligands. Furthermore, exploration of the spectroscopic properties of these complexes, particularly their vibrational spectra, provides model systems and benchmarks for interrogating the solution speciation of malonamide complexes in the organic phases in liquid-liquid extractions, where traditional techniques such as EXAFS and HEXS cannot provide the full picture.

Experimental Procedures

Synthetic Methods

All experimental solutions were prepared with methanol (VWR Chemicals BDH, ACS Grade, ≥99.8%) with 2-propanol (VWR Chemicals BDH, ACS Grade, ≥99.5%), ethanol (VWR Chemicals BDH, ≥95%), acetonitrile (Sigma-Aldrich, 99.8%), or tetrahydrofuran (EMPLURA, Extra Pure, Supelco) used as a co-solvent during crystallization. Lanthanum, cerium(III), praseodymium, neodymium, erbium, ytterbium nitrate salts and ammonium cerium(IV) nitrate were obtained from Sigma-Aldrich (99.9% metal basis), while samarium, europium, gadolinium, dysprosium, holmium, thulium, and lutetium nitrate salts were obtained from Strem Chemicals (99.9% metal basis). N,N,N',N'-tetramethylmalonamide was obtained from TCI America at >97.0% purity. All chemicals were used directly from the supplier without further purification.

Synthesis of Ln(*trans*-TMMA)$_2$(NO$_3$)$_3$ Ln = La, Ce, Pr, Nd, Sm

1.0 ml of 0.1M stock solution of $Ln(NO_3)_3 \bullet 6(H_2O)$ in methanol was added to the bottom of a 20 ml glass scintillation vial with subsequent layering of 2 ml of either methanol, ethanol, 2-propanol, acetonitrile, or tetrahydrofuran. On top of the experimental mixture 0.2 ml / 0.6 ml / 1.0 ml of 0.5M stock solution of N,N,N',N'-tetramethylmalonamide (TMMA) in methanol was layered depending on the desired Ln : TMMA molar ratio of 1:1, 1:3, or 1:5, respectively. The experimental vial was left in the chemical hood uncapped to slowly evaporate over time. The highest quality crystals of **Ln(*trans*-TMMA)$_2$(NO$_3$)$_3$** appeared at the bottom of the scintillation vial for the Ln : TMMA molar ratio of 1:3 and with 2-propanol as a co-solvent. The nature of lanthanide salts used in the reaction had significant impact on crystallization time with La crystallizing within 5 minutes and Sm crystallizing within 5 hours of the setup.

Synthesis of Ln(*cis*-TMMA)$_2$(NO$_3$)$_3$ Ln = Eu, Gd, Tb, Er

1.0 ml of 0.1M stock solution of $Ln(NO_3)_3 \bullet 6(H_2O)$ in methanol was added to the bottom of a 20 ml glass scintillation vial with subsequent layering of 2 ml of either methanol, ethanol, 2-propanol, acetonitrile, or tetrahydrofuran. On top of the experimental mixture 0.2 ml / 0.6 ml / 1.0 ml of 0.5M stock solution of N,N,N',N'-tetramethylmalonamide (TMMA) in methanol was layered depending on the desired Ln : TMMA molar ratio of 1:1, 1:3, or 1:5, respectively. Due to increasing hygroscopicity of lanthanide salts, the vials were left in the container filled with indicating drierite desiccant under a constant flow of nitrogen gas to minimize the exposure to moisture and promote crystallization. Similarly, the highest quality crystals of **Ln(*cis*-TMMA)$_2$(NO3)$_3$** appeared at the bottom of the scintillation vial for the Ln : TMMA molar ratio of 1:3 and with 2-propanol as a co-solvent.

Synthesis of [Ln(K^2-TMMA)$_2$(K^1-TMMA)(NO$_3$)$_2$][Ln(K^2-TMMA)(NO$_3$)$_4$] Ln = Dy, Ho

1.0 ml of 0.1M stock solution of $Ln(NO_3)_3 \bullet 6(H_2O)$ in methanol was added to the bottom of a 20 ml glass scintillation vial with subsequent layering of 2 ml of 2-propanol. On top of the experimental mixture 0.6 ml of 0.5M stock solution of N,N,N',N'-tetramethylmalonamide (TMMA) in methanol was layered

resulting in Ln : TMMA molar ratio of 1:3. The experimental vials were placed in the vacuum desiccator filled with indicating drierite and the headspace was evacuated to avoid any exposure to moisture. Hygroscopic, high quality crystals of **$[Ln(K^2\text{-}TMMA)_2(K^1\text{-}TMMA)(NO_3)_2][Ln(K^2\text{-}TMMA)(NO_3)_4]$** were formed in the bottom of the vials following several days of the setup.

Synthesis of $[Ln(K^2\text{-}TMMA)_2(K^1\text{-}TMMA)(NO_3)_2][Ln(K^2\text{-}TMMA)(K^1\text{-}NO_3)(NO_3)_3]$ Ln = Er, Tm

1.0 ml of 0.1M stock solution of $Ln(NO_3)_3 \bullet 5(H_2O)$ in methanol was added to the bottom of a 20 ml glass scintillation vial with subsequent layering of 2 ml of 2-propanol. On top of the experimental mixture 0.6 ml of 0.5M stock solution of N,N,N',N'-tetramethylmalonamide (TMMA) in methanol was layered resulting in Ln : TMMA molar ratio of 1:3. The experimental solutions were first evaporated under a steady stream of dry nitrogen gas overnight until thick clear oil was formed at the bottom of the vials, which was then placed in the vacuum desiccator filled with indicating drierite and the headspace was evacuated to avoid any exposure to moisture. Hygroscopic, high quality crystals of **$[Ln(K^2\text{-}TMMA)_2(K^1\text{-}TMMA)(NO_3)_2][Ln(K^2\text{-}TMMA)(K^1\text{-}NO_3)(NO_3)_3]$** were formed within the clear oil overnight.

Synthesis of $Ln(K^2\text{-}TMMA)(iPrOH)(NO_3)_3$ Ln = Yb, Lu

1.0 ml of 0.1M stock solution of $Ln(NO_3)_3 \bullet 5(H_2O)$ in methanol was added to the bottom of a 20 ml glass scintillation vial with subsequent layering of 2 ml of 2-propanol. On top of the experimental mixture 0.2 ml of 0.5M stock solution of N,N,N',N'-tetramethylmalonamide (TMMA) in methanol was layered resulting in Ln : TMMA molar ratio of 1:1. Following complete slow evaporation of the solution under the constant dry nitrogen gas flow, the vial containing thick clear oil was capped and stored. After 2-3 weeks clear crystals of **$Ln(K^2\text{-}TMMA)(iPrOH)(NO_3)_3$** formed in the bottom of the vial.

Synthesis of $Ln(K^2\text{-}TMMA)(K^1\text{-}TMMA)(NO_3)_3$ Ln = Yb, Lu

1.0 ml of 0.1M stock solution of $Ln(NO_3)_3 \bullet 5(H_2O)$ in methanol was added to the bottom of a 20 ml glass scintillation vial with subsequent layering of 2 ml of 2-propanol. On top of the experimental mixture 0.6 ml of 0.5M stock solution of N,N,N',N'-tetramethylmalonamide (TMMA) in methanol was layered

resulting in Ln : TMMA molar ratio of 1:3. The experimental vials were placed in the vacuum desiccator filled with indicating drierite and the headspace was evacuated to avoid any exposure to moisture. Hygroscopic, high quality crystals of **Ln(K^2-TMMA)(K^1-TMMA)(NO_3)$_3$** were formed in the bottom of the vials following several days of the setup.

X-ray Diffraction

The crystals of various Ln-TMMA complexes were removed from mother liquor and placed directly into the Parabar 10312 (Hampton Research) cryoprotective immersion oil. A high-quality single crystal of each compound was isolated on a tip of a glass fiber mounted on a Bruker Quazar single crystal diffractometer equipped with a microfocus X-ray beam (Mo Kα; λ = 0.71073 Å) and an Apex II detector. The crystallographic frames were collected at 100K (Oxford Cryosystems Cryostream 700) with the Bruker APEXII software package. Peak intensities were corrected for Lorentz, polarization, background effects, and absorption effects using the APEX3 software. Initial structure solution was determined by intrinsic phasing and refined on the basis of F^2 for all unique data using the SHELXL version 5 program. H atoms were placed with a riding model for all of the organic functional groups. Summaries of the crystallographic refinements are provided in the Supporting Information. Individual CIFs including the structure factors have been deposited with the Cambridge Crystallographic Data Center under accession codes 2296291-2296295 for Ln(*trans*-TMMA)$_2$(NO3)$_3$, 2296300-2296304 for Ln(*cis*-TMMA)$_2$(NO3)$_3$, 2296305, 2296306 for [Ln(K^2-TMMA)$_2$(K^1-TMMA)(NO_3)$_2$][Ln(K^2-TMMA)(NO_3)$_4$], 2296307, 2296308 for [Ln(K^2-TMMA)$_2$(K^1-TMMA)(NO_3)$_2$][Ln(K^2-TMMA)(K^1-NO_3)(NO_3)$_3$], 2296309, 2296311 for Ln(K^2-TMMA)(iPrOH)(NO_3)$_3$, and 22960310, 22960312 for Ln(K^2-TMMA)(K^1-TMMA)(NO_3)$_3$.

Powder X-ray diffraction patterns were collected on a Scintag diffractometer using nickel-filtered Cu Kα radiation (λ = 1.5418 Å), voltage 40 kV and current 40 mA. Samples were ground to fine powders using a mortar and pestle and run using zero background silica sample holder. Powder diffraction patterns were collected within the scan range of 5–50° 2θ and step size of 0.05°. and an exposure time of 1 second.

Vibrational Analysis

Solid-state compounds were analyzed by Fourier transform infrared (FT-IR) and Raman spectroscopy. FT-IR spectra were collected on an ATR accessory of a Nicolet Nexus 850 FT-IR spectrometer from 400-4000 cm^{-1} with a resolution of 2 cm^{-1}. Approximately 10-20 mg of the crystalline material was transferred directly into the ATR cavity and pressed down with the sampling arm.

Raman spectra were collected on a Renishaw inVia confocal Raman microscope with a Leica DM2700 series microscope using a 785 nm laser with a 1200/mm grating and a 532 nm laser with 2400/mm grating and a CCD detector. Each sample was isolated, mounted to a glass slide, and loaded onto the sample stage. Laser power was set at 10% (~50 mW) and the spectra were collected in the 100-1300 cm^{-1} range with each sample irradiated for an integration time of 1 second and automatically reiterated 100 times. Extended Raman scans were performed in the range 100-2000 cm^{-1} using variable laser power 10-50% with 10 seconds exposure time and 3-5 reiterations.

Computational Details

To identify the experimental IR and Raman spectra, we have performed auxiliary DFT calculations on selective crystal structures. Noting that organometallic complexes in this work consist of 200 atoms per unit cell, it is not achievable to run the calculations on the entire periodic crystal structures. Instead, we isolated each organometallic complex and ran the calculations for the cluster in gas phase. Although this significantly reduced computational cost, the isolated cluster is still composed of more than 50 atoms. Thus, we skipped geometry optimizations and ran the IR and Raman analysis on the cluster structures directly from XRD experiments. Because optimization of cluster structures in the gas phase without confinement may result in molecular structures that are different from those of the crystals, such a strategy can also prevent us from getting different structures from XRD experiments.

We used B3LYP level of theory for all the calculations, which has shown great alignment with experimental IR and Raman spectra for the organometallic system.[14] The Stuttgart/Dresden relativistic small-core (RSC) effective core potential (ECP) basis set,[15] obtained from Basis Set Exchange, was used

for Ln(III),[16] while the Dunning/Huzinaga full double-zeta basis set was used for other elements in the complex.[17] All DFT calculations were performed in Gaussian 16.[18]

Results and Discussion

Ln(*trans*-TMMA)$_2$(NO$_3$)$_3$

The first group of isostructural solid-state compounds involved early lanthanides La-Sm coordinated by two bidentate K^2-N,N,N',N'-tetramethylmalonamide ligands, as well as three nitrato ligands resulting in a charge neutral 10-coordinate complex, as shown in **Figure 1**. The Ln-O$_{TMMA}$ are equivalent across all structures with average distances ranging from 2.4897 Å to 2.4335 Å, while the Ln-O$_{nitrato}$ distances are typically elongated measuring from 2.6455 Å down to 2.5864 Å going from La to Sm, respectively. Going across the early lanthanide series, the bond distances for Ln-O$_{TMMA}$ and Ln-O$_{nitrato}$ gradually shorten by 0.017 Å and 0.018 Å respectively, correlating to the changes in the ionic radius.[19] Despite low symmetry of the metal complex, the spatial arrangement of malonamide ligands about the lanthanide metal center is best described as a *trans* conformation, with both TMMA ligands located on the opposite sides of the nitrate ligand belt. Quantifying the bite angle is challenging as the TMMA ligand is not planar, but it can be estimated by the angle between the methylene carbons of the ligands through the metal center, which measured to 128° for all La-Sm TMMA complexes. Overall, the Ln(*trans*-TMMA)$_2$(NO3)$_3$ is consistent with reported structures for lanthanum and neodymium by Parks *et al*, while the bulk crystalline material shows great agreement with calculated patterns for all La-Sm compounds (**Figure S19**).[7b]

It is worth noting a curious case of using ammonium cerium(IV) nitrate in the experimental prep, which still results in the isolation of Ce(III)(*trans*-TMMA)$_2$(NO$_3$)$_3$ crystals within 20 minutes of the setup with the experimental solution changing color from deep red-orange to clear during crystallization. The redox behavior of Ce(IV) in organic media is not unusual, as the salts of Ce(IV) have been used as homogeneous oxidants in organic synthesis for quite some time.[20] We first monitored the intensity of

Ce(IV) ligand-to-metal charge transfer band (A_{max} = ~270 nm) in pure methanol via UV-Vis in the absence of the malonamide ligand and we did not note any changes in the band intensity on the crystallization time scale (10-20 minutes), as shown in **Figure S29**. However, if the experiment is repeated in the presence of N,N,N',N'-tetramethylmalonamide at 1:1 metal to ligand ratio, we observe a rapid drop in intensity of the Ce(IV) LMCT within the first 5 minutes, with subsequent ingrowth of a weak absorption band at A_{max} = 260 cm^{-1} indicating the presence of Ce(III). The rapid reduction of Ce(IV) happens in ethanol media in about 37 minutes, yet TMMA ligand seems to be extremely prone to oxidation in the presence of Ce(IV), resulting in a full ingrowth of Ce(III) in just 7-8 minutes.[21]

In addition to X-ray diffraction results, we conducted an in-depth vibrational analysis on the crystals of Ln(*trans*-TMMA)$_2$(NO3)$_3$ Ln = La, Ce, Pr, Nd, Sm based on the obtained IR Raman spectra (**Figure 1B**), complemented by DFT frequency analysis to aid with vibrational band assignments. The IR

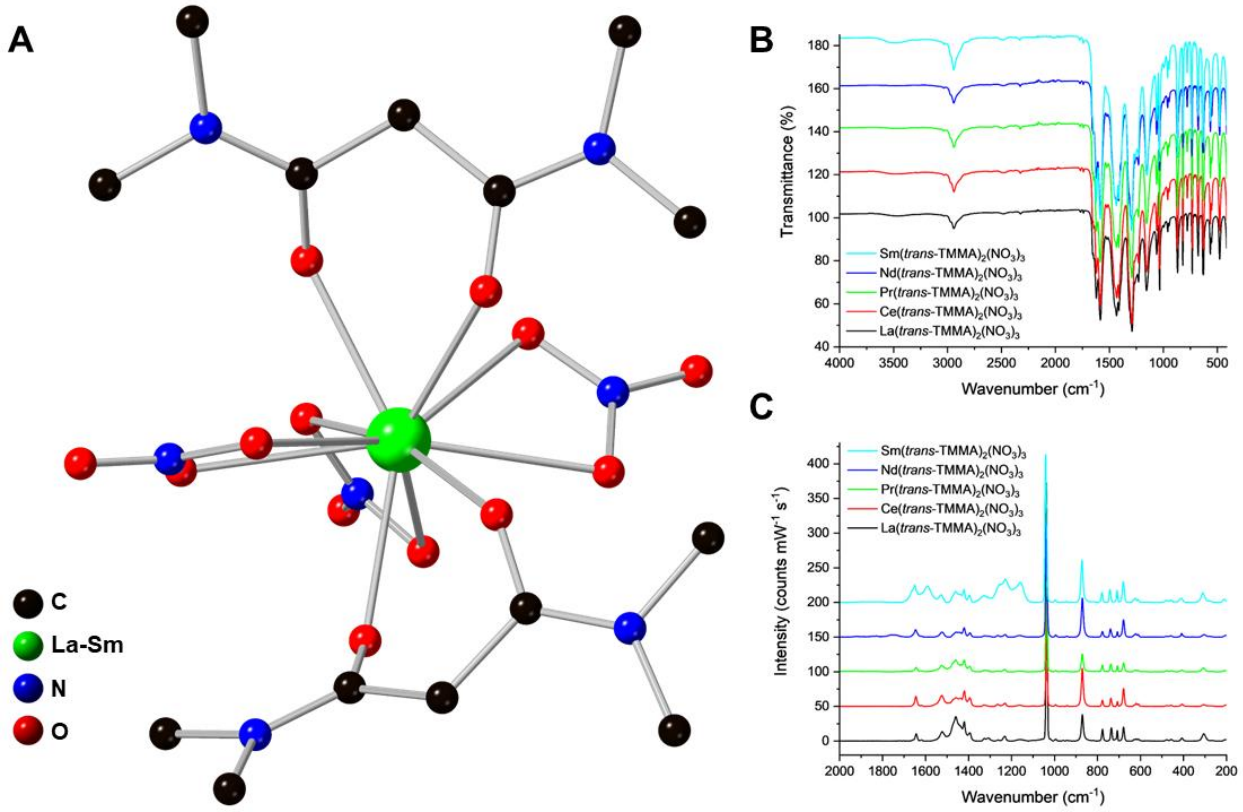

Figure 1. (**A**) Crystal structure of the Ln(*trans*-TMMA)$_2$(NO3)$_3$ complex isostructural for La-Sm; (**B**) ATR-IR spectra of the Ln(*trans*-TMMA)$_2$(NO3)$_3$ complexes; (**C**) Extended Raman spectra of the Ln(*trans*-TMMA)$_2$(NO3)$_3$ complexes.

and Raman spectra of the isostructural series display nearly identical peak positions; thus the following band assignments coincide for all La-Sm complexes. The IR spectrum of Ln(*trans*-TMMA)$_2$(NO3)$_3$ is dominated by a strong doublet centered at 1621 cm^{-1} and 1583 cm^{-1} in the C=O stretching region (amide I region). The stretching frequency of the amide C=O can be diagnostic of the variable ligand arrangement around the metal center, so we employed DFT frequency analysis in order to be more precise with our assignments. DFT calculations showed that the strong band at 1583 cm^{-1} corresponds to the C=O stretches that are out-of-phase with each other on the TMMA ligand, as well as out-of-phase with C=O stretching motion on the opposing ligand. The band at 1621 cm^{-1} was the result of individual carbonyl groups stretching in-phase with each other on a given ligand, while the two opposing TMMA ligands are overall out-of-phase with each other. The following region from 1390-1470 cm^{-1} was challenging to deconvolute due to the presence of several ν_3 NO_3^- assymmetric stretching modes (1451 cm^{-1}, 1470 cm^{-1}), the deformations of the O=C-CH$_2$-C=O backbone coupled to the C=O stretching (1413 cm^{-1}, 1434 cm^{-1}), as well as the symmetric N-CH$_3$ stretching on the amide (1390 cm^{-1}). Due to the presence of multiple amide functionalities across two ligands, expected amide bands were identified at 1263 cm^{-1} (amide III, ν O=C-N), 630 cm^{-1} (amide IV, N-C=O def), 564 cm^{-1} and 553 cm^{-1} (amide VI, out-of-plane N-C=O def).

The Raman spectrum of Ln(*trans*-TMMA)$_2$(NO3)$_3$ shows a prominent peak at 1038 cm^{-1} corresponding to the ν_1 symmetric stretching of the NO_3^-, which can also be visible in the IR spectrum at 1035 cm^{-1}. The vibrational modes of coordinated nitrate also show up in the Raman spectrum at 736 cm^{-1} (IR 731 cm^{-1}) and 680 cm^{-1} (IR 677 cm^{-1}) corresponding to the ν_6 and ν_5 stretching modes, respectively. Weak bands at 1307 cm^{-1} and 1328 cm^{-1} could be assigned to the in-plane bending mode of NO_3^- (IR 1304 cm^{-1}), while a medium intensity band at 1460 cm^{-1} is in the range of ν_3 asymmetric stretch of nitrate. The Raman region 600-900 cm^{-1} is mostly occupied by both symmetric and asymmetric modes of the C-N-C ligand backbone (e.g. 871 cm^{-1} and 778 cm^{-1}), as well as the out-of-plane bending of the dimethyl substituted amide (708 cm^{-1}). Interestingly, the Raman spectrum also captured low-energy Ln-O vibrations for both Ln-O_2NO and Ln-O_{TMMA} in the range of 100-200 cm^{-1} that are well-aligned with the

literature values. The rest of the assignments for both the IR and the Raman spectra are summarized in **Table 1.**

Table 1. IR and Raman bands of Ln(*trans*-TMMA)$_2$(NO3)$_3$ Ln = La, Ce, Pr, Nd, Sm.

IR	Raman	DFT	Assignment	Reference
	104 (w)		ν Ln-O_2NO	Bünzli *et al*[22]
	127 (vw)	122	$\nu_{\text{out-of-phase}}$ Ln-O=C	DFT
	161 (m)	173	$\nu_{\text{out-of-phase}}$ Ln-O=C	DFT
	201 (vw)		ν Ln-O_2NO	Bünzli *et al*[22]
	211 (vw)		ν Ln-O_2NO	Bünzli *et al*[22]
405 (s)	408 (w)	407	ρ C-C skeletal	DFT
	457 (w)	456	ω N-CH_3	DFT
476 (m)	478 (w)		ν C-C skeletal	Socrates[23]
553 (sh, w)			Amide VI, out-of-plane N-C=O def	Socrates[23]
564 (m)			Amide VI, out-of-plane N-C=O def	Socrates[23]
630 (s)			Amide IV, N-C=O def	Bellamy[24]
677 (m)	680 (m)		ν_5 NO_3	Bünzli *et al*[22]
	708 (m)	698	$\delta_{\text{out-of-plane}}$ H_3C-N-CH_3	DFT
731 (s)	736 (m)		ν_6 NO_3	Bünzli *et al*[22]
778 (w)	778 (m)		ν_{asym} C-N-C	Socrates[23]
822 (m)			ν_2 NO_3 out-of-plane bend	Bünzli *et al*[22]
867 (s)	871 (m)		ν_{sym} C-N-C	Socrates[23]
944 (sh, vw)			δ CH_2	De Beukeleer and Desseyn[25]
960 (w)			δ CH_2	De Beukeleer and Desseyn[25]
1035 (s)	1038 (vs)		ν_1 NO_3 symmetric stretch	Bünzli *et al*[22]
1060 (m)			δ CH_3	Socrates[23]
1156 (s)			ν_{asym} O=C-CH_2-C=O backbone	Socrates[23]
1230 (sh, m)	1229 (w)		ν_4 NO_3 in-plane bend	Bünzli *et al*[22]
1263 (sh, m)			Amide III, ν O=C-N	Bellamy[24]
1291 (vs)			ν_4 NO_3 in-plane bend	Rapko *et al*[8]
1304 (sh, s)	1307 (w)		ν_4 NO_3 in-plane bend	Rapko *et al*[8]
	1328 (w)		ν_4 NO_3 in-plane bend	Rapko *et al*[8]
1390 (sh, m)	1393 (w)		ν N-CH_3	Bellamy[24]
1412 (s)	1421 (m)	1428	O=C-CH_2-C=O def coupled to ν C=O	DFT
1434 (vs)	1437 (sh)	1438	O=C-CH_2-C=O def coupled to ν C=O	DFT
1451 (sh, s)	1460 (m)		ν_3 NO_3 asymmetric stretch	Rapko *et al*[8]
1470 (sh, m)			ν_3 NO_3 asymmetric stretch	Rapko *et al*[8]
1583 (vs)	1522 (m)	1589	$\nu_{\text{out-of-phase}}$ C=O	DFT
1621 (s)	1619 (vw)	1623	$\nu_{\text{in-phase}}$ C=O, *trans*-TMMA out-of-phase	DFT
1645 (sh, m)	1643 (m)	1649	$\nu_{\text{in-phase}}$ C=O, *trans*-TMMA in-phase	DFT

2942 (w)	ν C-H (CH_2)	Bellamy[24]
2976 (w)	ν C-H (CH_3)	Bellamy[24]

Ln(*cis*-TMMA)$_2$(NO$_3$)$_3$

The contraction of europium, gadolinium, terbium, and erbium brought about ligand rearrangement around the metal center in crystallized complexes of these lanthanides with N,N,N',N'-tetramethylmalonamide, resulting in the isolation of a second structural group of compounds. The bidentate binding mode of both diamide ligands was preserved, yet the TMMA ligands were now grouped together in the same coordinating hemisphere, while three bidentate nitrato ligands were aggregated on the opposing side of the lanthanide metal, still resulting in a charge-neutral complex (**Figure 2A**). The isostructural compounds in this series were designated as *cis* conformers, resulting in an overall formula of Ln(*cis*-TMMA)$_2$(NO$_3$)$_3$, as evidenced by a decreasing C-Ln-C bite angle between two TMMA ligands ranging from 73° to 107°, compared to the 128° for the Ln(*trans*-TMMA)$_2$(NO$_3$)$_3$ conformers. A gradually decreasing Ln-O$_{TMMA}$ bond distance was noted across the new isostructural series ranging from 2.3959 Å (Eu) down to 2.3349 Å (Er), in conjunction with slightly elongated Ln-O$_{nitrato}$ distances of 2.5585 - 2.5113 Å, paralleling the trend observed for Ln(*trans*-TMMA)$_2$(NO$_3$)$_3$.

Synthesis and isolation of Ln(*cis*-TMMA)$_2$(NO$_3$)$_3$ Ln = Eu, Gd, Tb, Er was not as straightforward as the early lanthanide counterparts, due to the increase in hydration enthalpy of these lanthanides, resulting in the formation of hygroscopic complexes. In case of gadolinium, we additionally isolated a dihydrate Gd(*cis*-TMMA)$_2$(NO$_3$)$_3$ • 2H$_2$O analogue, which showed a much tighter grouping of the N,N,N',N'-tetramethylmalonamide ligands with the bite angle of 72.89° compared to the anhydrous complex at 106.99°. Despite settle difference in the unit cell parameters and the bite angles of the ligands, the Ln(*cis*-TMMA)$_2$(NO$_3$)$_3$ complexes are consistent for the middle lanthanides (Eu, Gd, Tb) with the Er being the only late lanthanide that crystallized out under the same synthetic conditions. Interestingly, Parks *et al*. reported the structure for Eu(TMMA)$_2$(NO$_3$)$_3$ as the *trans* conformer, suggesting that the

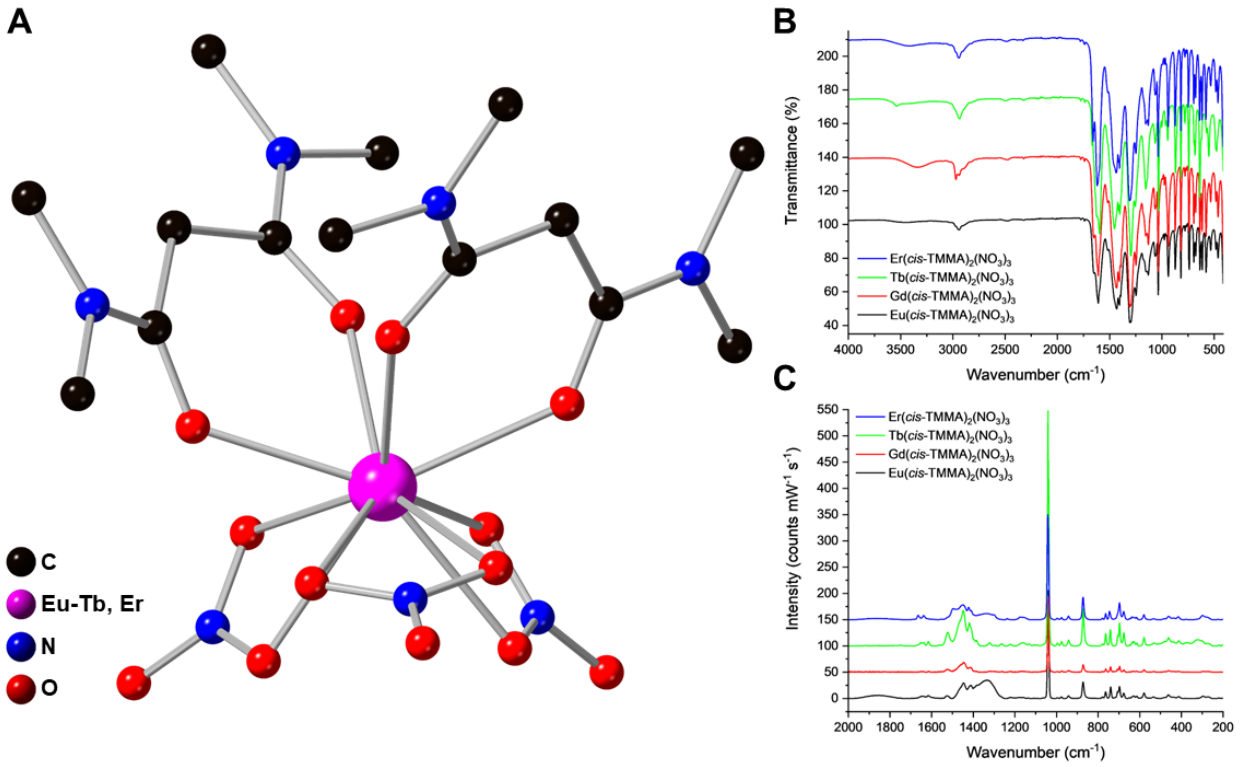

Figure 2. (**A**) Crystal structure of the Ln(*cis*-TMMA)$_2$(NO3)$_3$ complex for Eu, Gd, Tb, Er; (**B**) ATR-IR spectra of the Ln(*cis*-TMMA)$_2$(NO3)$_3$ complexes; (**C**) Extended Raman spectra of the Ln(*cis*-TMMA)$_2$(NO3)$_3$ complexes.

ligand rearrangement into the *cis* isomer occurs starting at gadolinium.[7b] In our case, we report isolation of the Eu(*cis*-TMMA)$_2$(NO$_3$)$_3$ compound and further confirm the prevalence of the Eu-*cis*-TMMA complex by checking the bulk crystalline purity of the solid-state material based on the experimental and calculated powder X-ray diffraction patterns. It appears that such amphoteric behavior of europium is highly dependent on the solvent system used during the synthesis of the solid-state compounds.

The infrared spectrum of Ln(*cis*-TMMA)$_2$(NO$_3$)$_3$ is similar to the Ln(*trans*-TMMA)$_2$(NO$_3$)$_3$ discussed above with noticeable frequency shifts in the carbonyl stretching region, nitrate bending region, as well as the skeletal vibrations of the diamide ligand (**Figure 2B**). The strongest vibrational features associated with the C=O stretches of Ln(*cis*-TMMA)$_2$(NO$_3$)$_3$ show up at 1610 cm^{-1} with a shoulder at 1653 cm^{-1} corresponding to the in-phase stretching of two carbonyl functional groups on the same ligand, while being either out-of-phase or in-phase across the neighboring TMMA ligands, respectively. Both bands are shifted by ± 10 cm^{-1} compared to the Ln(*trans*-TMMA)$_2$(NO$_3$)$_3$ compound, though it was

surprising to observe the disappearance of the ν_{asym} C=O bands from the infrared spectrum of Ln(*cis*-TMMA)$_2$(NO$_3$)$_3$. The following intense vibrational bands at 1434 cm^{-1} and 1307 cm^{-1} aligned with ν_3 asymmetric stretching and ν_4 in-plane bending modes of the nitrate ligands, accompanied by the strong peak at 1035 cm^{-1} assigned to the ν_1 symmetric stretching of the NO_3^-. We did note the appearance of new vibrational modes associated with asymmetric stretching of the O=C-CH$_2$-C=O backbone (1130 cm^{-1}) and the disubstituted amide C-N-C (693 cm^{-1}), among several other weaker skeletal modes, yet the rest of the vibrations were well-aligned with Ln(*trans*-TMMA)$_2$(NO$_3$)$_3$.

The complexity and significant peak overlap in the infrared spectrum made it challenging to compare the vibrational modes between the *trans* and the *cis* conformers, but these differences are somewhat noticeable within the Raman spectra of these compounds. The Raman spectrum of Ln(*cis*-TMMA)$_2$(NO$_3$)$_3$ is dominated by the band centered at 1041 cm^{-1} with a prominent shoulder at 1038 cm^{-1}, both corresponding to the ν_1 stretching of the nitrate anion, in contrast with the singular 1038 cm^{-1} band for the *trans* conformer (**Figure 2B**). The Raman spectra share some similarities in bands located at 871 cm^{-1} (ν_{sym} C-N-C), 741 cm^{-1} (ν_6 NO$_3$), and 676 cm^{-1} (ν_5 NO$_3$), yet the skeletal vibrations such as ν_{asym} and ν_{sym} C-N-C appearing at 697 cm^{-1} and 764 cm^{-1} only appear in the Ln(*cis*-TMMA)$_2$(NO$_3$)$_3$ series, making it possible to distinguish the conformers via vibrational spectroscopy. The detailed summary of the remainder of the IR and Raman band assignments can be found in **Table S5** in the Supporting Information section.

[Ln(TMMA)$_3$(NO$_3$)$_2$][Ln(TMMA)(NO$_3$)$_4$]

Increasing hygroscopicity of the complexes containing the metals from the second half of the lanthanide series prompted us to use vacuum desiccators to ensure crystallization of the Ln-TMMA compounds. This synthetic approach allowed us to isolate an unusual structural family of compounds consisting of anion-cations pairs of N,N,N',N'-tetramethylmalonamide complexes with Dy, Ho, Er, and Tm. As shown in **Figure 3A 3C**, the cationic complex on the left includes a 9-coordinate Ln(III) metal center (Dy-Tm) bound to two bidentate (K^2-TMMA) and one monodentate (K^1-TMMA) malonamide

ligands, along with two bidentate nitrato ligands, resulting in an overall +1 charge of the complex. In case of Dy and Ho, the counter-anion is composed of a 10-coordinate Ln(III) with a single bidentate (K^2-TMMA) diamide ligand and four bidentate (K^2-NO_3) nitrato ligands, resulting in an overall formula of $[Ln(K^2\text{-TMMA})_2(K^1\text{-TMMA})(NO_3)_2][Ln(K^2\text{-TMMA})(NO_3)_4]$, with a mixed 9/10-coordinate Ln = Dy, Ho. While the molecular cation for Er and Tm has an identical coordination environment, the counter-anion is comprised of a 9-coordinate Ln(III) metal center bound with three bidentate (K^2- NO_3) and one monodentate (K^1- NO_3) nitrato ligands and a single bidentate (K^2-TMMA) diamide ligand giving an overall formula of $[Ln(K^2\text{-TMMA})_2(K^1\text{-TMMA})(NO_3)_2][Ln(K^2\text{-TMMA})(K^1\text{-}NO_3)(NO_3)_3]$ Ln = Er, Tm. The metal-oxo distances once again followed the contraction trend with Ln-O_{TMMA} shortening from 2.3229 Å (Dy) to 2.2896 Å (Tm), and Ln-$O_{nitrato}$ measuring from 2.4926 Å (Dy) down to 2.4437 Å (Tm). The exception being the Ln-O bond length for the monodentate nitrato ligand within the Er and Tm

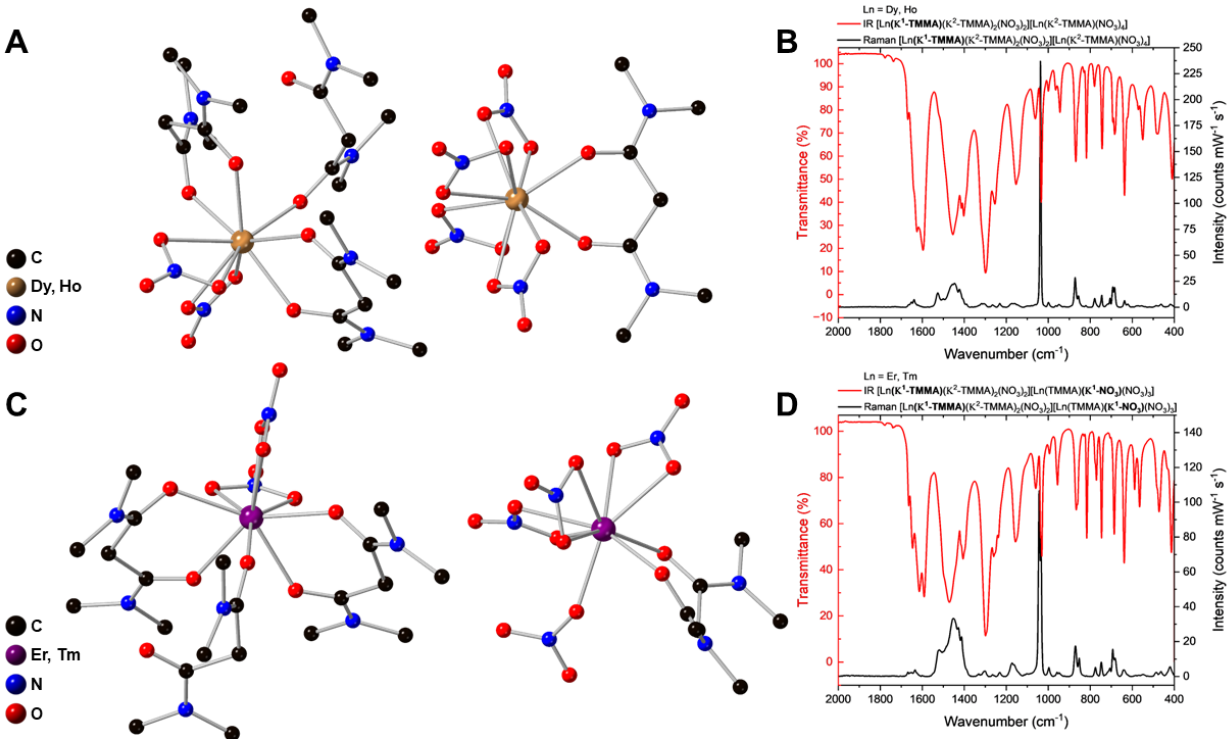

Figure 3. (**A**) Crystal structure of the $[Ln(K^2\text{-TMMA})_2(K^1\text{-TMMA})(NO_3)_2][Ln(K^2\text{-TMMA})(NO_3)_4]$ complex for Dy and Ho; (**B**) ATR-IR and Raman spectra of the $[Ln(K^2\text{-TMMA})_2(K^1\text{-TMMA})(NO_3)_2][Ln(K^2\text{-TMMA})(NO_3)_4]$ Ln = Dy, Ho complexes; (**C**) Crystal structure of the $[Ln(K^2\text{-TMMA})_2(K^1\text{-TMMA})(NO_3)_2][Ln(K^2\text{-TMMA})(K^1\text{-}NO_3)(NO_3)_3]$ complex for Er and Tm; (**D**) ATR-IR and Raman spectra of the $[Ln(K^2\text{-TMMA})_2(K^1\text{-TMMA})(NO_3)_2][Ln(K^2\text{-TMMA})(K^1\text{-}NO_3)(NO_3)_3]$ Ln = Er, Tm complexes

compounds measuring at 2.297 Å and 2.258 Å, respectively, which is ~0.17 Å shorter than the typical Ln-$O_{nitrato}$ distance for those complexes.

Isolation of lanthanide and actinide complexes as the anion-cation pairs in the solid state is quite common, especially with neutral ligands used in separation sciences, such as diglycolamides. Typically, the neutral polydentate diamides fully saturate the lanthanide(III) metal center, and the resulting homoleptic +3 molecular cation is charge balanced by a lanthanide(III) hexanitrato complex, as demonstrated by Duval *et al*.[26] The same behavior has been observed in low-valent actinide complexes with diglycolamides as well.[27] However, there are only a few reported examples of compounds that include heteroleptic anion-cation pairs with trivalent lanthanides (La, Nd, Tb, Yb) and neutral/zwitterionic polydentate ligands.[28] In case of malonamides, there are no examples of reported heteroleptic anion-cation pairs with the exception of $[Dy(K^2\text{-TMMA})_2(K^1\text{-TMMA})(NO_3)_2][Dy(K^2\text{-TMMA})(NO_3)_4]$, which has been published within Crystallographic Structural Database (2044462).

The increase in structural complexity of the $[Ln(TMMA)_3(NO_3)_2][Ln(TMMA)(NO_3)_4]$ further complicated the vibrational analysis of these compounds. The carbonyl stretching region 1550-1700 cm^{-1} is rather similar between the Dy/Ho-TMMA and Er/Tm-TMMA anion-cation pairs with slight shifts in the vibrational frequencies, as seen on **Figure 3B 3D**. Overall, the strongest vibrational band for both subsets of compounds is located at 1591-1596 cm^{-1} region and corresponds to the out-of-phase C=O stretching of the bidentate TMMA ligand, followed by a strong band in the 1613 cm^{-1} assigned to the in-phase C=O stretch of the bidentate K^2-TMMA coupled to the stretching of the uncoordinated C=O of the monodentate K^1-TMMA. The remaining bands typically show up as shoulder peaks in the 1624-1668 cm^{-1} range and signify combination modes of both in- and out-of-phase motions of the carbonyl group across mono- and bidentate TMMA ligands.

The major structural difference between the two subsets of compounds is the presence of a monodentate K^1-NO_3 nitrato ligand on the Er/Tm-TMMA molecular anion. Although it is not possible to unambiguously distinguish the nitrate denticity on the IR spectra alone, the splitting of the ν_1 and ν_3

modes of NO_3^- can be used as a criterion for this purpose. The frequency assigned to the asymmetric NO_3^- stretching is to intense signals at 1456 cm^{-1} (Dy/Ho-TMMA) and 1470 cm^{-1} (Er/Tm-TMMA), however the deconvolution of these bands is challenging due to significant broadening, thus masking the distinction between K^1-NO_3 and K^2-NO_3. Inspecting the ν_1 symmetric NO_3^- stretching region in the IR is more helpful as the single band at 1034 cm^{-1} for Dy/Ho-TMMA splits into two bands located at 1031 cm^{-1} and 1036 cm^{-1} for Er/Tm-TMMA complex. Interestingly, the complimentary Raman spectra also show that the sharp 1038 cm^{-1} band (ν_1 NO_3^- Dy/Ho-TMMA) splits into three new bands at 1035 cm^{-1}, 1039 cm^{-1}, and 1044 cm^{-1} (Er/Tm-TMMA) suggesting a change in the coordination environment of the nitrato ligands.[29] Last but not the least, characteristic features of the monodentate vs. bidentate coordination modes of NO_3^- are weak intensity bands near 1750 cm^{-1}, assigned to the combination modes that could be used for structural diagnosis, as suggested by Curtis and Curtis.[30] If the frequency difference (Δ) between the nitrato $\nu_1 + \nu_4$ combination modes, which commonly show up as weak doublets, falls around ~30 cm^{-1}, the bidentate coordination mode is assigned, while the frequency difference of about ~10 cm^{-1} suggests a monodentate binding.[31] For example, the IR spectrum of Dy/Ho-TMMA displays two weak resonances at 1737 cm^{-1} and 1777 cm^{-1} with $\Delta = 40$ cm^{-1} indicating only the K^2-NO_3 coordination, while the IR spectrum of Er/Tm-TMMA shows weak bands at 1779 cm^{-1}, 1740 cm^{-1}, and 1732 cm^{-1} with $\Delta = 39$ cm^{-1} and $\Delta = 8$ cm^{-1} confirming the presence of both K^1-NO_3 and K^2-NO_3.

Ln(K^2-TMMA)(iPrOH)(NO_3)$_3$ and Ln(K^1-TMMA)(K^2-TMMA)(NO_3)$_3$

The last group of coordination compounds was isolated out of reactions of N,N,N',N'-tetramethylmalonamide with ytterbium and lutetium nitrates, where the identity of the crystalline material was affected by both the metal-to-ligand molar ratio and the organic co-solvent used during crystallization, unlike the previously discussed compounds. First, we isolated the 9-coordinate charge-neutral Ln(K^2-TMMA)(iPrOH)(NO_3)$_3$ Ln = Yb, Lu complex out of the reaction with Ln : TMMA = 1 : 1 stoichiometry and 2-propanol as a co-solvent, resulting in a Yb/Lu metal center bound by a single malonamide ligand in a bidentate fashion, three bidentate nitrato ligands, and a molecule of isopropanol

completing the coordination sphere (**Figure 4A**). The average Ln-O_{TMMA} distances ranged at 2.2490 Å (Yb) - 2.2460 Å (Lu), with slightly elongated Ln-$O_{nitrato}$ distances at 2.4112 Å (Yb) and 2.4022 Å (Lu) and Ln-O_{iPrOH} distance of ~2.295 Å for the coordinated isopropanol, falling in line with the expected trends for lanthanide contraction overall. If the same reaction is carried out in the absence of 2-propanol and at elevated molar ratios of Ln : TMMA = 1 : 3, the lanthanide metal center is coordinated by one bidentate K^2-TMMA and one monodentate K^1-TMMA, along with three bidentate NO_3^- ligands, once again resulting in a charge-neutral 9-coordinate Ln(K^1-TMMA)(K^2-TMMA)$(NO_3)_3$ Ln = Yb, Lu complex (**Figure 4B**). The Ln-O_{TMMA} distances for Ln(K^1-TMMA)(K^2-TMMA)$(NO_3)_3$ are 2.2267 Å (Yb) and 2.2230 Å (Lu), slightly shorter compared to the isopropanol analogue, while Ln-$O_{nitrato}$ are relatively

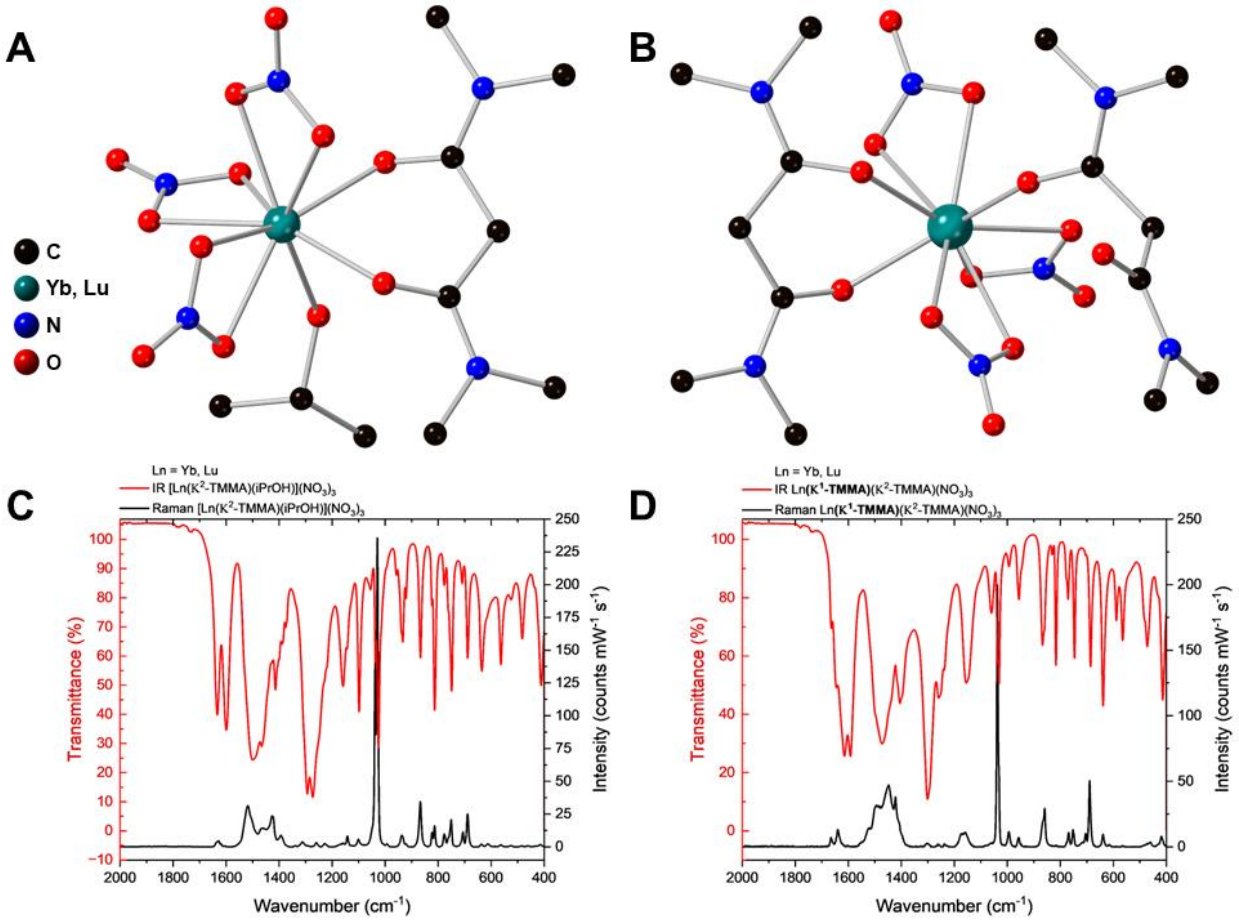

Figure 4. (**A**) Crystal structure of the Ln(K^2-TMMA)(iPrOH)$(NO_3)_3$ Ln = Yb, Lu; (**B**) Crystal structure of the Ln(K^1-TMMA)(K^2-TMMA)$(NO_3)_3$ Ln = Yb, Lu; (**C**) ATR-IR and Raman spectra of the Ln(K^2-TMMA)(iPrOH)$(NO_3)_3$; (**D**) ATR-IR and Raman spectra of the Ln(K^1-TMMA)(K^2-TMMA)$(NO_3)_3$.

longer at 2.430 Å (Yb) and 2.4193 Å (Lu). Across multiple experimental attempts, it appears that presence of any amount of 2-propanol in the reaction of ytterbium or lutetium nitrates with N,N,N',N'-tetramethylmalonamide, regardless of the molar ratio, results in TMMA ligand displacement and crystallization of Ln(K^2-TMMA)(iPrOH)(NO_3)$_3$ compound, suggesting rather weak coordination of diamides to the late lanthanides. Interestingly, Den Auwer *et al.* reported a similar structure of the Yb/Lu-N,N,N′,N′-tetraethylmalonamide (ethyl disubstituted amide), where both TEMA ligand are coordinated via K^2 mode to the metal center, along with two bidentate K^2-NO_3 and one monodentate K^1-NO_3.[32] The switch in denticity from the malonamide to the nitrato ligand is unclear, especially due to similarities in preparation of the complex (ethanol/2-propanol vs. methanol/2-propanol solvent mixture).

Vibrational spectra of Ln(K^2-TMMA)(iPrOH)(NO_3)$_3$ and Ln(K^1-TMMA)(K^2-TMMA)(NO_3)$_3$ display noticeable differences, mostly due to the coordinated isopropanol and variable number of complexed TMMA ligands, as shown in **Figures 4C 4D**. The carbonyl stretching region for Ln(K^2-TMMA)(iPrOH)(NO_3)$_3$ was significantly less convoluted compared to the other complexes discussed above with just two frequencies at 1599 cm^{-1} and 1634 cm^{-1} corresponding to the $\nu_{out\text{-}of\text{-}phase}$ and $\nu_{in\text{-}phase}$ C=O stretching of the diamide ligand, both coupled to the ν_3 NO_3, according to our DFT calculations. In contrast, the spectrum of the Ln(K^1-TMMA)(K^2-TMMA)(NO_3)$_3$ shows numerous features in the 1550-1700 cm^{-1} region due to the combination modes of in- and out-phase carbonyl stretching across two TMMA ligands with different coordination modes. Another major difference between the two subgroups of compounds stemmed from the vibrational signatures of the 2-propanol highlighted by a broad band at 3306 cm^{-1} characteristic to the O-H stretching of the alcohol functionality, as well as a sharp feature at 1098 cm^{-1} of the C-O stretch.

Additionally, there are some discrepancies in the vibrational features associated with the NO_3^- anions, specifically in the shifts and the splitting of the ν_1 and ν_4 vibrational modes. The IR spectrum of Ln(K^2-TMMA)(iPrOH)(NO_3)$_3$ shows two strong resonances for ν_4 NO_3 in-plane bend at 1273 cm^{-1} and 1294 cm^{-1} along with two sharp peaks for ν_1 NO_3 symmetric stretch at 1024 cm^{-1} and 1036 cm^{-1}. The ν_1

NO_3 symmetric stretch resonance at 1031 cm^{-1} and ν_4 NO_3 in-plane bend at 1301 cm^{-1} in the IR spectrum of Ln(K^1-TMMA)(K^2-TMMA)$(NO_3)_3$, both appear to split into two resonances at 1024 cm^{-1} and 1036 cm^{-1} in the case of ν_1 NO_3, as well as 1273 cm^{-1} and 1294 cm^{-1} in the case of ν_4 NO_3 of Ln(K^2-TMMA)(iPrOH)$(NO_3)_3$. This behavior is also highlighted when cross-examining the ν_1 NO_3 signal in the Raman spectra for both compounds where the single band at 1038 cm^{-1} is split into 1029 cm^{-1} and 1039 cm^{-1}. Comparing the solid-state structures of two compounds may explain this discrepancy due to a different nitrato ligand arrangement around the lanthanide metal center, where Ln(K^2-TMMA)(iPrOH)$(NO_3)_3$ displays grouping of nitrate ligands in the same coordinating hemisphere resembling the Ln(*cis*-TMMA)$_2(NO_3)_3$ conformer, while the arrangement of Ln(K^1-TMMA)(K^2-TMMA)$(NO_3)_3$ resembled the Ln(*trans*-TMMA)$_2(NO_3)_3$ conformer.

Relevance To Liquid-Liquid Separations

Understanding trends in structural chemistry of the metal-malonamide model complexes across the entire lanthanide series may provide insight in the chemical behavior of the rare-earth metals during liquid-liquid separations. The reports on lanthanide-actinide extraction within the scope of the DIAMEX-SANEX process mostly focus on the use of N,N′-dimethyl-N,N′-dioctylhexylethoxymalonamide (DMDOHEMA) as the diamide-based extractant. For example, Chiarizia *et al*. determined the distribution ratios of lanthanides at the concentrations of ≥0.04M with 0.7M DMDOHEMA in *n*-dodecane from 1M HNO_3 and 2M $LiNO_3$ aqueous solution, as shown in **Figure 5** (digitized and recompiled using WebPlotDigitizer).[1] It is evident that the D values decrease significantly while moving across the lanthanide series. The decline in D values is typically explained by the increase in steric hindrance caused by trying to accommodate three nitrate ions and bulky malonamide ligands around a shrinking metal cation. Therefore, a deeper understanding of the potential coordination geometries and ligand arrangement around the Ln is necessary to understand separations behavior in these extraction systems.

While solution behavior often deviates from solid state coordination by homolog ligands of the extractant, structural information on Ln-TMMA complexes across the entire lanthanide series helps us

further clarify the D value groupings in the context of extraction experiments discussed above, if we assume that the crystalized lanthanide compounds conserve their structure in solution. The highest recorded distribution ratios appear for La-Nd in the range from 7.5 and 8.0, with Sm being slightly lower at $D_{Sm} = 6.1$, all corresponding to the Ln(*trans*-TMMA)$_2$(NO$_3$)$_3$ structure. Interestingly, after this series of relatively high and consistent D values, the drop in D for the heavier lanthanides coincides with the structural changes found in the solid state. After Sm, we observe a stepwise drop off in the distribution ratios for Eu, Gd, and Tb which generally crystallize out as Ln(*cis*-TMMA)$_2$(NO$_3$)$_3$ conformer, where presence of any interstitial water molecules greatly affects the bite angle of the diamide ligands. The subsequent decrease of D values for Dy-Tm tetrad can be accounted for by the formation of heteroleptic Ln-TMMA anion-cation pairs, making it difficult to extract into an aliphatic solvent such as *n*-dodecane, unlike charge-neutral molecular complexes before. While we do not anticipate the extraction of these Lns in the form of such ions pairs, this behavior is suggestive of the relative instability of extractable (neutral)

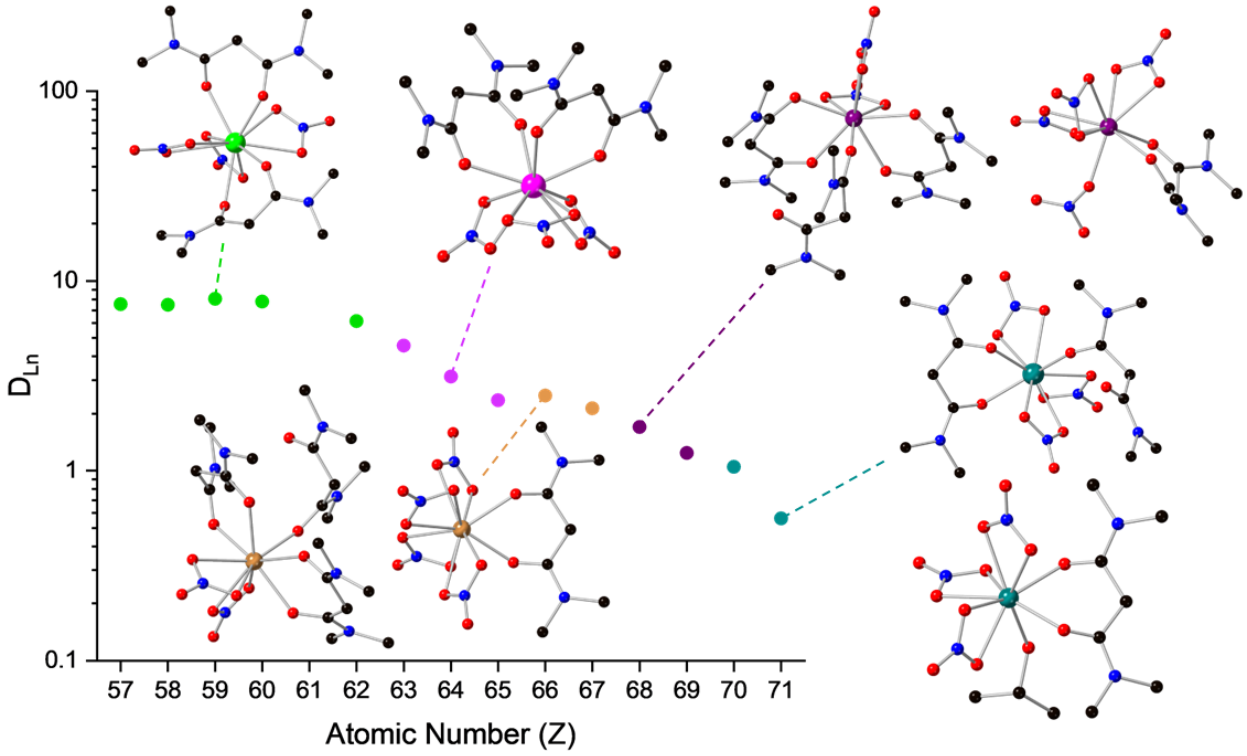

Figure 5. Distribution ratios of lanthanide ions from Chiarizia *et al*. for the extraction by 0.7M DMDOHEMA in *in*-dodecane from 1M HNO$_3$ – 2M LiNO$_3$ at 23 °C. The plot is color coded and overlayed with crystal structures of corresponding Ln-TMMA model compounds.

complexes. Finally, the lowest D values were recorded for ytterbium and lutetium, despite both metals forming a charge-neutral Ln(K^1-TMMA)(K^2-TMMA)$(NO_3)_3$ compound. We hypothesize that in the case of Yb and Lu weakly bound diamide ligands can be readily displaced by solvent molecules, as observed in Ln(K^2-TMMA)(iPrOH)$(NO_3)_3$ with the coordination of 2-propanol, specifically water molecules due to more favorable hydration enthalpies of the late lanthanides.

Conclusion

A series of reactions between lanthanide nitrate salts and N,N,N′,N′-tetramethylmalonamide resulted in isolation of four distinct groups of model compounds with variable ligand arrangement about the metal center, denticity of the coordinated ligand, and supramolecular assembly of charged molecular complexes across the entire lanthanide period. The structural trends across the four groups of coordination compound were carefully evaluated and compared to similar structures reported in the literature. Overall, the change in coordination arrangement of ligands was noted for early-middle lanthanides (La-Tb) due to the decrease in ionic radius of the metal center, while later lanthanides (Dy-Tm) additionally showed the formation of rare heteroleptic anion-cation pairs, instead of charge neutral complexes. Extensive vibrational investigation was performed on every structure via both IR and Raman spectroscopy, along with DFT frequency analysis, allowing to compare and contrast unique vibrational signatures associated with each structure type. The structural trends across the lanthanide series were also discussed in context of distribution ratios within liquid-liquid separations.

References

[1] B. Gannaz, R. Chiarizia, M. R. Antonio, C. Hill, G. Cote, *Solvent Extraction and Ion Exchange* **2007**, *25*, 313-337.

[2] L. Berthon, J. M. Morel, N. Zorz, C. Nicol, H. Virelizier, C. Madic, *Separation Science and Technology* **2001**, *36*, 709-728.

[3] X. Heres, E. Ameil, I. Martinez, P. Baron, C. Hill, *Extractant separation in DIAMEX-SANEX process*, American Nuclear Society - ANS, United States, **2007**.

[4] H. C. Aspinall, *Chemistry of the f-Block Elements*, Taylor & Francis, **2001**.

[5] D. Jańczewski, D. N. Reinhoudt, W. Verboom, E. Malinowska, M. Pietrzak, C. Hill, C. Allignol, *New Journal of Chemistry* **2007**, *31*, 109-120.

[6] G. Sandrone, D. A. Dixon, B. P. Hay, *The Journal of Physical Chemistry A* **1999**, *103*, 3554-3561.

[7] aG. J. Lumetta, B. M. Rapko, P. A. Garza, B. P. Hay, R. D. Gilbertson, T. J. R. Weakley, J. E. Hutchison, *Journal of the American Chemical Society* **2002**, *124*, 5644-5645; bB. W. Parks, R. D. Gilbertson, J. E. Hutchison, E. R. Healey, T. J. R. Weakley, B. M. Rapko, B. P. Hay, S. I. Sinkov, G. A. Broker, R. D. Rogers, *Inorganic Chemistry* **2006**, *45*, 1498-1507.
[8] B. M. Rapko, B. K. McNamara, R. D. Rogers, G. J. Lumetta, B. P. Hay, *Inorganic Chemistry* **1999**, *38*, 4585-4592.
[9] L. Spjuth, J. O. Liljenzin, M. J. Hudson, M. G. B. Drew, P. B. Iveson, C. Madic, *Solvent Extraction and Ion Exchange* **2000**, *18*, 1-23.
[10] M. J. Servis, M. Piechowicz, S. Skanthakumar, L. Soderholm, *Physical Chemistry Chemical Physics* **2021**, *23*, 8880-8890.
[11] G. Y. S. Chan, M. G. B. Drew, M. J. Hudson, P. B. Iveson, J.-O. Liljenzin, M. Skålberg, L. Spjuth, C. Madic, *Journal of the Chemical Society, Dalton Transactions* **1997**, 649-660.
[12] E. E. Castellano, R. W. Becker, *Acta Crystallographica Section B* **1981**, *37*, 1998-2001.
[13] S. Kannan, G. Ferguson, *Inorganic Chemistry* **1997**, *36*, 1724-1725.
[14] C. Lee, W. Yang, R. G. Parr, *Physical Review B* **1988**, *37*, 785-789.
[15] X. Cao, M. Dolg, *Journal of Molecular Structure: THEOCHEM* **2002**, *581*, 139-147.
[16] B. P. Pritchard, D. Altarawy, B. Didier, T. D. Gibson, T. L. Windus, *Journal of Chemical Information and Modeling* **2019**, *59*, 4814-4820.
[17] T. H. Dunning, P. J. Hay, H. Schaefer, *Modern theoretical chemistry* **1977**, *3*, 1-28.
[18] M. J. Frisch, G. W. Trucks, H. B. Schlegel, G. E. Scuseria, M. A. Robb, J. R. Cheeseman, G. Scalmani, V. Barone, G. A. Petersson, H. Nakatsuji, X. Li, M. Caricato, A. V. Marenich, J. Bloino, B. G. Janesko, R. Gomperts, B. Mennucci, H. P. Hratchian, J. V. Ortiz, A. F. Izmaylov, J. L. Sonnenberg, Williams, F. Ding, F. Lipparini, F. Egidi, J. Goings, B. Peng, A. Petrone, T. Henderson, D. Ranasinghe, V. G. Zakrzewski, J. Gao, N. Rega, G. Zheng, W. Liang, M. Hada, M. Ehara, K. Toyota, R. Fukuda, J. Hasegawa, M. Ishida, T. Nakajima, Y. Honda, O. Kitao, H. Nakai, T. Vreven, K. Throssell, J. A. Montgomery Jr., J. E. Peralta, F. Ogliaro, M. J. Bearpark, J. J. Heyd, E. N. Brothers, K. N. Kudin, V. N. Staroverov, T. A. Keith, R. Kobayashi, J. Normand, K. Raghavachari, A. P. Rendell, J. C. Burant, S. S. Iyengar, J. Tomasi, M. Cossi, J. M. Millam, M. Klene, C. Adamo, R. Cammi, J. W. Ochterski, R. L. Martin, K. Morokuma, O. Farkas, J. B. Foresman, D. J. Fox, Wallingford, CT, **2016**.
[19] V. Goldschmidt, *Oslo I, Mat-Naturvidensk Kl* **1926**, *8*.
[20] W. S. Trahanovsky, L. B. Young, G. L. Brown, *The Journal of Organic Chemistry* **1967**, *32*, 3865-3868.
[21] V. Briois, D. Lützenkirchen-Hecht, F. Villain, E. Fonda, S. Belin, B. Griesebock, R. Frahm, *The Journal of Physical Chemistry A* **2005**, *109*, 320-329.
[22] J.-C. G. Bünzli, E. Moret, J.-R. Yersin, *Helvetica Chimica Acta* **1978**, *61*, 762-771.
[23] G. Socrates, *Infrared and Raman Characteristic Group Frequencies: Tables and Charts*, Wiley, **2004**.
[24] L. J. Bellamy, *The Infrared Spectra of Complex Molecules: Volume Two Advances in Infrared Group Frequencies*, Springer Netherlands, **1980**.
[25] S. H. J. De Beukeleer, H. O. Desseyn, *Spectrochimica Acta Part A: Molecular Spectroscopy* **1994**, *50*, 2291-2309.
[26] S. Kannan, M. A. Moody, C. L. Barnes, P. B. Duval, *Inorganic Chemistry* **2008**, *47*, 4691-4695.
[27] B. M. Rotermund, J. M. Sperling, G. P. Horne, N. B. Beck, H. B. Wineinger, Z. Bai, C. Celis-Barros, D. Gomez Martinez, T. E. Albrecht-Schönzart, *Inorganic Chemistry* **2023**, *62*, 12905-12912.
[28] aM. G. B. Drew, D. Guillaneux, M. J. Hudson, P. B. Iveson, C. Madic, *Inorganic Chemistry Communications* **2001**, *4*, 462-466; bM. Frechette, C. Bensimon, *Inorganic Chemistry* **1995**, *34*, 3520-3527; cL. Xu, Y.-F. Ma, K.-Z. Tang, Y. Tang, W.-S. Liu, M.-Y. Tan, *Journal of Fluorescence* **2008**, *18*, 685-693; dM. Nakase, T. Kobayashi, H. Shiwaku, S. Suzuki, T. S. Grimes, B. J. Mincher, T. Yaita, *Solvent Extraction and Ion Exchange* **2018**, *36*, 633-646; eP. Delangle, C.

Husson, C. Lebrun, J. Pécaut, P. J. A. Vottéro, *Inorganic Chemistry* **2001**, *40*, 2953-2962; fF. H. Barnes, A. W. Kelly, H. Melzer, H. H. Patterson, R. D. Pike, *Zeitschrift für anorganische und allgemeine Chemie* **2018**, *644*, 525-533.
[29] M. Y. Mihaylov, V. R. Zdravkova, E. Z. Ivanova, H. A. Aleksandrov, P. S. Petkov, G. N. Vayssilov, K. I. Hadjiivanov, *Journal of Catalysis* **2021**, *394*, 245-258.
[30] N. F. Curtis, Y. M. Curtis, *Inorganic Chemistry* **1965**, *4*, 804-809.
[31] A. B. P. Lever, E. Mantovani, B. S. Ramaswamy, *Canadian Journal of Chemistry* **1971**, *49*, 1957-1964.
[32] C. Den Auwer, M. C. Charbonnel, M. G. B. Drew, M. Grigoriev, M. J. Hudson, P. B. Iveson, C. Madic, M. Nierlich, M. T. Presson, R. Revel, M. L. Russell, P. Thuéry, *Inorganic Chemistry* **2000**, *39*, 1487-1495.